Journal of Inflammation Research

Dovepress
Taylor & Francis Group

Open Access Full Text Article

ORIGINAL RESEARCH

MALAT1's m^{6}A Modification by METTL3 Promotes Pyroptosis and Inflammation in Sepsis-Induced Acute Kidney Injury in Mice

Pengwei Guo[1,*], Gao Deng[1,*], Lingling Li[1], Haidong Wei[1], Yunxia Gong[1], Yanhong Tan[1], Yanfei Ma[2]

[1]Department of Nephrology, Affiliated Hospital of Youjiang Medical University for Nationalities, Baise City, Guangxi Zhuang Autonomous Region, People's Republic of China; [2]Department of Glandular Surgery, Affiliated Hospital of Youjiang Medical University for Nationalities, Baise City, Guangxi Zhuang Autonomous Region, People's Republic of China

*These authors have contributed equally to this work

Correspondence: Yanfei Ma, Department of Glandular Surgery, Affiliated Hospital of Youjiang Medical University for Nationalities, No. 18, Zhongshan 2nd Road, Baise City, Guangxi Zhuang Autonomous Region, People's Republic of China, Email yanfei.ma@ymun.edu.cn

Background: Sepsis-induced acute kidney injury (SAKI) significantly contributes to renal dysfunction. Long non-coding RNA MALAT1 has been implicated in regulating inflammation and cell death in various diseases. However, its role in SAKI and the underlying mechanisms remain unclear.

Methods: A lipopolysaccharide (LPS)-induced SAKI mouse model and LPS-treated TCMK-1 cells were established. METTL3 and MALAT1 were manipulated via lentiviral-mediated knockdown or overexpression. m6A RNA levels were measured using MeRIP-qPCR, while pyroptosis and inflammation were assessed through ELISA, flow cytometry, Western blotting, immunohistochemistry, and immunofluorescence. RNA immunoprecipitation was conducted to confirm the interaction between METTL3 and MALAT1.

Results: LPS treatment significantly increased METTL3 and MALAT1 expression and enhanced m^{6}A modification of MALAT1. METTL3 knockdown reduced pyroptosis markers (cleaved GSDMD, Caspase-1, and NLRP3) and inflammatory cytokines (IL-1β and IL-18), while MALAT1 overexpression partially reversed these effects. RIP confirmed that METTL3 binds directly to MALAT1. In vivo and in vitro experiments demonstrated that the METTL3/MALAT1 axis contributes to pyroptosis in SAKI.

Conclusion: METTL3 promotes pyroptosis in SAKI by enhancing the m6A modification of MALAT1. Targeting the METTL3/MALAT1 axis may provide a potential therapeutic strategy for SAKI by mitigating renal inflammation and cell death.

Keywords: sepsis-induced acute kidney injury, METTL3, MALAT1, pyroptosis

Introduction

Sepsis, a life-threatening condition triggered by infection, involves complex physiological, pathological, and biochemical abnormalities.[1] Sepsis-induced acute kidney injury (SAKI) is a prevalent complication that significantly contributes to the high morbidity and mortality rates in sepsis cases.[2] Survivors of SAKI are at a heightened risk of developing chronic kidney disease, underscoring its lasting clinical effects.[3] Despite the urgent clinical need, no effective therapies for SAKI currently exist, emphasizing the importance of understanding its pathogenesis to develop targeted treatment strategies.

While SAKI is typically defined by severe kidney dysfunction-characterized by elevated blood urea nitrogen and serum creatinine levels-histological analyses often reveal only mild tubular injury with minimal evidence of classical necrosis.[4] This discrepancy suggests that regulated forms of cell death other than necrosis may play key roles in SAKI pathogenesis.[5,6] Among these, pyroptosis-a form of programmed cell death characterized by caspase-1 activation, gasdermin D (GSDMD) cleavage, and the release of inflammatory cytokines such as IL-1β and IL-18-has recently garnered significant attention.[7–9] In sepsis and AKI models, elevated pyroptosis has been implicated in promoting renal inflammation and injury.[10] However, the regulatory mechanisms driving pyroptosis in SAKI remain incompletely understood.

Received: 24 March 2025
Accepted: 29 September 2025
Published: 24 October 2025

Long non-coding RNAs (lncRNAs), transcripts longer than 200 nucleotides that do not code for proteins, are emerging as key regulators of gene expression in various diseases, including AKI.[11,12] Among them, metastasis-associated lung adenocarcinoma transcript 1 (MALAT1) has been shown to influence inflammatory responses and cell death in kidney injury. Previous studies demonstrated that MALAT1 knockdown alleviated AKI through modulation of miRNA signaling pathways, such as the miR-204/APOL1/NF-κB and MALAT1/miR-205 axes.[13–15] More recently, MALAT1 has also been implicated in regulating pyroptosis in non-renal diseases, including liver fibrosis and viral myocarditis.[16,17] However, whether MALAT1 modulates pyroptosis in SAKI remains unclear.

Epigenetic modifications, particularly RNA methylation, have gained attention as potential modulators of lncRNA function. Among the over 100 RNA modifications identified, N6-methyladenosine (m^6A) is the most prevalent internal modification of eukaryotic mRNA and lncRNA.[18,19] m6A methylation is known to affect RNA splicing, stability, translation, and decay, thereby influencing gene expression post-transcriptionally. These modifications are dynamically regulated by "writers" (methyltransferases such as METTL3 and METTL14), "erasers" (demethylases such as FTO and ALKBH5), and "readers" (RNA-binding proteins such as YTHDFs and IGF2BPs).[20,21]

METTL3, the catalytic core of the m6A methyltransferase complex, has been extensively studied for its roles in cancer biology, stem cell differentiation, and immune regulation.[20,21] However, its role in kidney injury, particularly in the context of sepsis, remains poorly defined. Given that lncRNAs such as MALAT1 can undergo m6A methylation, and that METTL3 has been shown to modulate inflammation and cell death in other diseases, it is plausible that METTL3-mediated m6A modification may influence MALAT1's function in SAKI.

In this study, we aimed to investigate whether METTL3 regulates MALAT1 expression through m^6A methylation, and how this axis contributes to pyroptosis and inflammation in SAKI. Using an LPS-induced AKI mouse model and in vitro cellular assays, we examined the functional interactions between METTL3 and MALAT1 and assessed their roles in modulating renal inflammation and pyroptosis. Our findings provide new insights into the epigenetic regulation of lncRNAs in SAKI and suggest potential therapeutic targets involving METTL3 and MALAT1.

Methods

Establishment and Treatment of AKI Mouse Model

Clean-grade, healthy ICR mice (6–8 weeks old, 18–22 g) were used for all experiments. All experimental procedures were reviewed and approved by Zhuoqiang Biotechnology Co., Ltd. (Approval No.: zqia-2023-027). Animal care and use complied with the National Institutes of Health Guidelines for the Care and Use of Laboratory Animals and adhered to the Animal Research: Reporting of In Vivo Experiments guidelines.

Mice were housed in individually ventilated cages (IVCs) under standard laboratory conditions (temperature 25 ± 2 °C, relative humidity 60–80%, 12-h light/dark cycle) with free access to autoclaved food and water. Each cage housed no more than five mice, with sterilized corncob bedding and environmental enrichment (such as nesting material and shelters) provided to support animal welfare. All animals were acclimatized for one week prior to experimentation to reduce stress and ensure physiological stability.

A total of 60 mice were randomly assigned to experimental groups using a computer-generated randomization table To minimize bias, investigators responsible for treatment administration, sample collection, and outcome assessment were blinded to group allocations throughout the study.

SAKI was induced via intraperitoneal injection of lipopolysaccharide (LPS, from Escherichia coli O111:B4, Sigma-Aldrich, St. Louis, MO, USA; Cat. No. L2630) at a dose of 10 mg/kg body weight, diluted in sterile phosphate-buffered saline to a total volume of 500 μL per mouse. Control mice received an equal volume of sterile saline.

For genetic manipulation, lentiviral vectors carrying sh-MALAT1, sh-METTL3, or OE-MALAT1, along with corresponding negative control vectors (sh-NC, OE-NC), were administered via tail vein injection at a volume of 100 μL per mouse. A single intraperitoneal injection of LPS (10 mg/kg) was given 2 hours after lentiviral administration to induce AKI. No additional injections were performed. The experimental groups included: Control, AKI, AKI+sh-NC, AKI+sh-MALAT1, AKI+sh-METTL3, AKI+OE-NC (pc-MALAT1), AKI+OE-MALAT1 (pc-MALAT1), and AKI+sh-METTL3+OE-MALAT1 (pc-MALAT1).

At 24 hours post-modeling, mice were anesthetized and euthanized by cervical dislocation. Blood samples were collected via cardiac puncture and centrifuged to isolate serum, which was immediately aliquoted and stored at −80 °C until analysis. Kidney tissues were promptly harvested, rinsed with cold saline, and either fixed in 4% paraformaldehyde for histological examination or snap-frozen in liquid nitrogen and stored at -80 °C for molecular and biochemical assays.

Luminex Assay

Whole blood samples were collected via retro-orbital bleeding and allowed to clot at room temperature before centrifugation to isolate serum. Serum levels of creatinine and blood urea nitrogen (BUN) were quantified using a multiplex Luminex assay (Mouse Premixed Multi-Analyte Kit, LXSAMSM-05, R&D Systems, USA), according to the manufacturer's instructions. The assay was performed on a Luminex LX100 system (Luminex Corporation, USA), enabling simultaneous detection of multiple analytes. Measurements were recorded in μmol/L. All samples were analyzed in duplicate to ensure assay reliability.

Hematoxylin & Eosin (HE) Staining

Kidney tissues from each group were fixed in 4% paraformaldehyde for 24 h and processed into 4 μm paraffin sections. Sections were deparaffinized in xylene, rehydrated through graded ethanol, and stained with hematoxylin for 5 min. After washing, sections were differentiated with HCl-ethanol for 30 sec and counterstained with eosin for 2 min. After dehydration and clearing, slides were mounted and examined under a Nikon Eclipse E100 microscope (Nikon, Japan). Representative images were captured using a Nikon DS-Fi3 digital camera. Negative controls included omission of primary stain and replacement with saline.

ELISA (Enzyme-Linked Immunosorbent Assay)

Levels of IL-1β (EMC001b) and IL-18 (EMC011) in mouse serum and cell culture supernatants were measured using commercial ELISA kits (Neobioscience, China) according to the manufacturer's instructions. Standard curves were generated using provided standards. Positive controls were included as recommended by the kit, and blank wells without sample or antibody served as negative controls to account for background signal.

Cell Culture and LPS Treatment

TCMK-1 cells purchased from FuHeng Cell Center (Shanghai, China) are cultured in a medium supplemented with 10% fetal calf serum, 100 U/mL penicillin, and 100 μg/mL streptomycin, maintained at 37°C in a 5% CO_2 and 95% humidity incubator. TCMK-1 cells at passage 3 were exposed to LPS for 24 h to create a renal cell injury model. The STR profiling and mycoplasma testing reports for the TCMK-1 cell line are provided as an Additional File (see Supporting Information).

Cell Transfection

TCMK-1 cells were transfected with the following lentiviral constructs: sh-NC, sh-MALAT1, sh-METTL3, OE-NC, OE-MALAT1, sh-MALAT1+OE-NC, sh-METTL3+OE-MALAT1, and sh-NC+OE-NC. All lentiviral vectors were purchased from GeneChem (Shanghai, China) and validated for knockdown or overexpression efficiency. Transfections were performed using Lipofectamine 2000 (Thermo Fisher Scientific, Waltham, MA, USA) according to the manufacturer's protocol. Briefly, cells were seeded to achieve 70–80% confluence and transfected in serum-free DMEM medium. After 6 hours, the medium was replaced with complete medium, and cells were incubated at 37°C with 5% CO_2 for 48 hours prior to subsequent analyses.

RT-qPCR Detection

Total RNA was extracted with Trizol (Invitrogen, USA) and reverse transcribed into cDNA using an RT kit (Thermo, USA) following the manufacturer's instructions. Quantitative PCR was conducted using an ABI 7500 real-time instrument (ABI, Foster City, CA, USA) with the SYBR® Premix Ex Taq kit (Thermo, USA). The relative expression of each target gene was calculated using the $2^{-\Delta\Delta Ct}$ method, with GAPDH serving as the internal reference. No-template controls (NTC) and minus reverse transcriptase (−RT) controls were included to monitor for contamination and genomic DNA interference. Primers were synthesized by Sangon Biotech.

meRIP-qPCR Detection

Total RNA was extracted using Trizol, followed by fragmentation with a non-contact automatic ultrasonic disrupter at high power for 30 sec, repeated 30 times. Immunoprecipitation was performed with antibodies and magnetic beads for pretreatment. After combining with protein A/G, RNA was re-extracted, and cDNA synthesis was conducted using a first-strand cDNA synthesis kit as per the manufacturer's instructions. Using the SYBR® Premix Ex Taq™ II kit, RNA is extracted and fluorescence quantitative PCR is performed on a real-time PCR instrument (ABI 7500, ABI, Foster City, CA, USA). IgG pulldown served as a negative control to ensure specificity, and all experiments were repeated in triplicate. Primers were designed by Sangon.

Western Blotting

Protein samples were extracted by lysing TCMK-1 cells with RIPA buffer or homogenizing mouse kidney tissue, followed by quantification using a bicinchoninic acid (BCA) kit (Beyotime, Shanghai, China). Protein lysates were mixed with loading buffer (Beyotime), denatured at 100 °C for 5 minutes, and separated via SDS-PAGE. Electrophoresis was performed at 80 V for 30 min (stacking gel) and 120 V for 2 h (resolving gel), followed by wet transfer to PVDF membranes at 200 mA for 60–90 min in an ice bath.

Membranes were blocked with 5% BSA (Solarbio, Beijing, China) in TBST for 1 h at room temperature and incubated overnight at 4 °C with primary antibodies. The following primary antibodies were used: GAPDH (60004-1-Ig, 1:20,000), NGAL (30576-1-AP, 1:2000), KIM-1 (30,948-1-AP, 1:2000), Caspase-1 (31,020-1-AP, 1:1000), GSDMD (20770-1-AP, 1:2000), GSDMD-N (DF13758, Affinity, 1:5000), and NLRP3 (30,109-1-AP, 1:1000) (all from Proteintech unless otherwise specified). Membranes were then washed 5 times (10 min each) with TBST and incubated with HRP-conjugated secondary antibodies (1:5000, Beyotime) for 1 h at room temperature. Protein signals were detected using enhanced chemiluminescence (ECL kit, Servicebio, China) and visualized via a chemiluminescence imaging system.

Band intensities were quantified using ImageJ software (NIH, USA). Protein expression levels were normalized to GAPDH, which was chosen based on its established stability across inflammation and kidney injury models. A visible molecular weight marker (Western Protein Marker I, Cat. No. G2086, Servicebio) was used for reference. Negative controls included omission of the primary antibody to verify specificity. All Western blot experiments were performed in at least three independent biological replicates.

Determination of Pyroptosis by Flow Cytometry

To evaluate cell pyroptosis, flow cytometry was conducted using the FAM Fluorescent Dye-Labeled Caspase Inhibitor (FLICA) Caspase Detection Kit (ImmunoChemistry Technologies, LLC, USA), which utilizes a fluorescent inhibitor probe specific for active Caspase-1. Both TCMK-1 cells and kidney tissue-derived cells were assessed.

For in vitro analysis, TCMK-1 cells were treated with various conditions as described. After treatment, approximately 290 μL of cells (3×10^5 cells/mL) were transferred into fresh tubes and incubated with 10 μL of FAM-YVAD-FMK, a fluorescent-labeled caspase-1 inhibitor, at 37°C in the dark for 30 minutes. Cells were then stained with 1 μg/mL TMR red (C58-12156792910, Roche, USA) for 5 minutes to assess membrane integrity. After washing with PBS, samples were analyzed using a FACSCalibur flow cytometer (Becton Dickinson, Sunnyvale, CA). Cells double-positive for FAM-FLICA and PI were considered pyroptotic. Unstained cells, single-stained controls, and isotype controls were used for compensation and gating strategies.

For kidney tissue analysis, single-cell suspensions were prepared by enzymatic digestion of fresh kidney tissues using collagenase IV and DNase I, followed by filtration through a 70 μm cell strainer. The same FLICA and TMR red staining procedure as above was applied. Flow cytometric data were processed using FlowJo software (version X.0.7).

RNA Immunoprecipitation (RIP) Assay

RIP was performed using a modified polysome lysis-based protocol to examine the interaction between METTL3 and MALAT1. TCMK-1 cells were lysed in polysome lysis buffer (Beyotime, China) supplemented with protease inhibitor cocktail (Sigma-Aldrich, USA) and RNase inhibitor (Promega, USA), followed by DNA digestion with DNase I (Takara,

Japan) at 37 °C for 10 minutes. The lysate was clarified by centrifugation (16,000 g, 10 min, 4 °C), and supernatants were collected.

Protein A/G magnetic beads (Thermo Fisher Scientific, USA) were pre-washed and incubated with either anti-METTL3 antibody (ab195352, Abcam, UK) or normal rabbit IgG (Santa Cruz Biotechnology, USA) at 4 °C overnight. The antibody-bound beads were then incubated with 800 μL of cell lysates at 4 °C for 1 hour with rotation. After washing steps, the RNA-protein complexes were digested with proteinase K (Thermo Fisher Scientific, USA), and RNA was purified using phenol: chloroform: isoamyl alcohol (25:24:1, Sigma-Aldrich) extraction and ethanol precipitation.

Purified RNA was reverse-transcribed into cDNA using a PrimeScript™ RT reagent kit (Takara, Japan), and MALAT1 enrichment was analyzed by conventional PCR and qPCR with SYBR Green Master Mix (Vazyme, China). PCR products were visualized on 2% agarose gels, and relative enrichment was calculated using the %Input method.

Immunohistochemistry (IHC)

Immerse the prepared kidney tissue sections in boiling EDTA antigen retrieval buffer (pH 9.0) for 10 min to retrieve antigens. Following natural cooling, the sections underwent three PBS washes and a 10-min incubation with 3% hydrogen peroxide to inhibit endogenous peroxidase activity. Sections were washed thrice with PBS, sealed with serum for 30 min, and incubated overnight at 4°C with primary antibodies against Caspase-1 (31,020-1-AP), GSDMD-N (DF13758, Affinity), and NLRP3 (30,109-1-AP), each at a 1:500 dilution, using 50 μL of blocking solution. Sections were washed thrice in PBS and then incubated with secondary antibodies for 30 min at room temperature. Sections were washed thrice with PBS, stained with 3,3'-diaminobenzidine, followed by a 3 min hematoxylin stain, differentiated in 1% HCl-ethanol for 3 sec, and rinsed with running water. The sections were restored to blue using 0.6% ammonia water, followed by washing with running water, dehydration with graded ethanol, clearing with xylene, and sealing with neutral glue. Observe and photograph the sections with an ordinary light microscope. IHC scoring was conducted on a minimum of 100 cells across 10 randomly chosen fields using Image J software, followed by independent scoring by two experienced pathologists. The staining outcomes were assessed with the widely recognized German semi-quantitative scoring system by two blinded pathologists. Cell positivity was assessed by scoring the percentage of positive cells and staining intensity. Positive cell percentages were scored as: 0 for <5%, 1 for 5%-25%, 2 for 26%-50%, 3 for 51%-75%, and 4 for 76%-100%. Staining intensity was scored as: 0 for colorless, 1 for light yellow, 2 for brown, and 3 for tan. The overall positivity was determined by multiplying these scores: 0 indicates negative, 1–4 indicates weak positivity, 5–8 indicates positive, and 9–12 indicates strong positivity.[22] Imaging was performed using a Leica DM3000 LED light microscope (Leica Microsystems, Germany), and images were captured using the Leica DFC450 C camera. ImageJ was used for analysis, and scoring was conducted by two blinded pathologists. Isotype controls and omission of primary antibodies served as negative controls.

Immunofluorescence

Cells were fixed with 4% paraformaldehyde, permeabilized using 0.1% Triton at room temperature for 10 minutes, and blocked with 5% FBS. They were then incubated at 37°C for 1 h, followed by overnight incubation with primary antibodies including Caspase-1 (31,020-1-AP, 1:1000), GSDMD-N (DF13758, Affinity, 1:5000), and NLRP3 (30,109-1-AP, 1:1000) at 4°C. Incubate with secondary antibody at 37°C in the dark for 1 h, followed by a 15 min room temperature incubation with Hoechst in the dark. Negative controls included omission of primary antibody and use of isotype-matched IgG. Images were acquired using a Zeiss Axio Observer A1 fluorescence microscope (Carl Zeiss, Germany) and analyzed using ImageJ software.

Statistical Analysis

All statistical analyses were conducted using GraphPad Prism 8 (GraphPad Software, San Diego, CA, USA). Data are presented as mean ± standard deviation (SD).

Prior to analysis, the Shapiro–Wilk test was used to assess the normality of the data distribution. For data sets that followed a normal distribution, unpaired two-tailed Student's t-tests were used to compare two groups. For comparisons involving three or more groups, one-way or two-way analysis of variance (ANOVA) was performed depending on the

number of factors, followed by Tukey's multiple comparisons test for post hoc analysis. For data that did not meet the assumptions of normality, non-parametric alternatives such as the Mann–Whitney *U*-test or Kruskal–Wallis test with Dunn's post hoc test were applied. Correction for multiple comparisons was performed using Tukey's or Dunn's test depending on whether parametric or non-parametric analysis was used.

All biological experiments were independently repeated at least three times, with triplicate technical replicates for each condition unless otherwise specified. A P value < 0.05 was considered statistically significant.

Results

In the LPS-Induced AKI Mouse Model, Malat1 Upregulation Was Associated with Increased Pyroptosis and Impaired Renal Function

LPS-induced AKI in mice resulted in pronounced renal damage, inflammation, and pyroptosis. HE staining revealed substantial histological alterations in the AKI group, including tubular epithelial cell detachment, luminal dilation, and cytoplasmic vacuolation compared with the Control group (Figure 1A). ELISA analysis demonstrated that serum levels

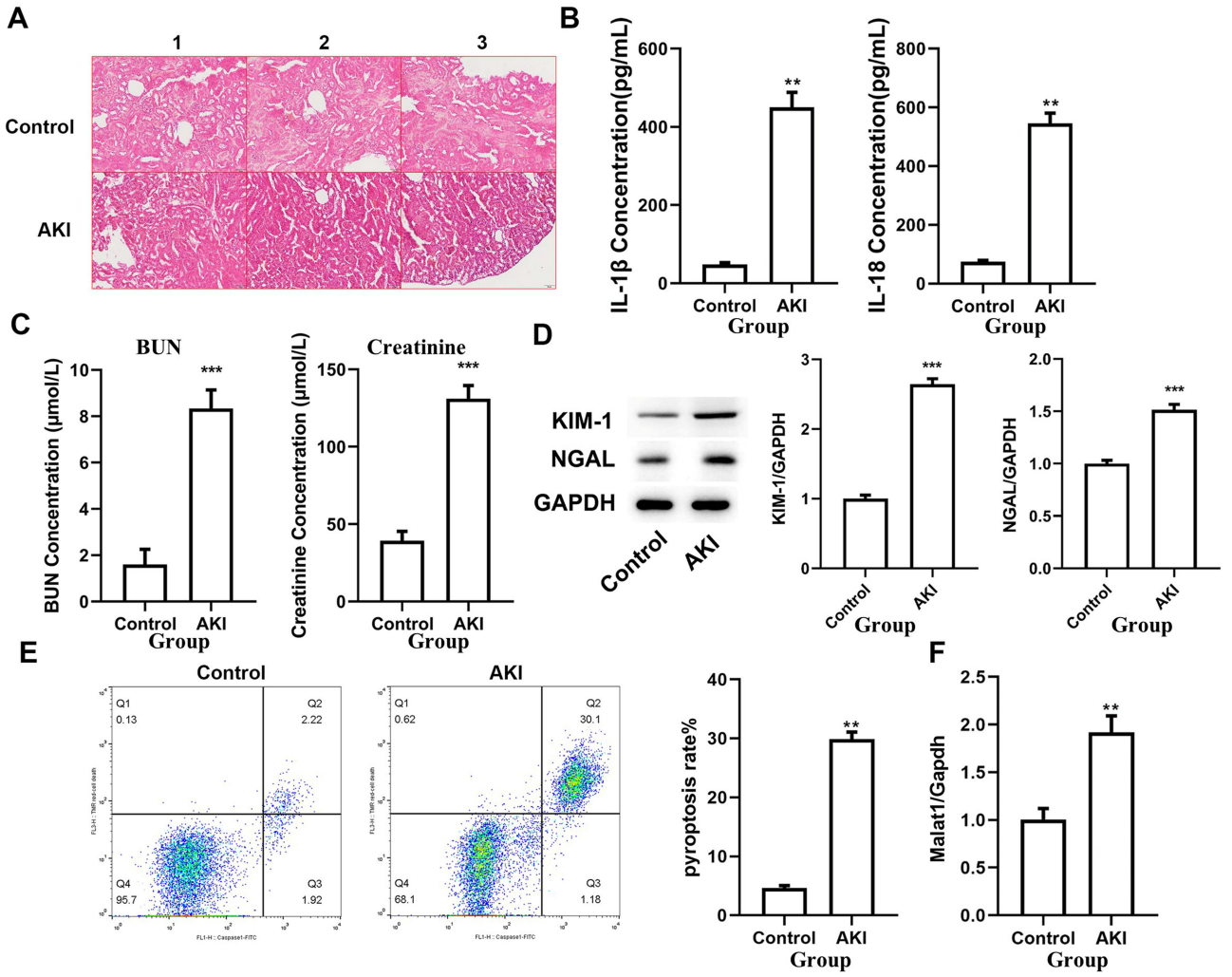

Figure 1 Evaluation of renal histopathology, function, inflammation, pyroptosis, and Malat1 expression in a mouse model of LPS-induced acute kidney injury (AKI). (**A**) HE staining of kidney tissue sections from control and AKI mice. (**B**) Quantification of serum pro-inflammatory cytokines IL-1β and IL-18 by ELISA. (**C**) Assessment of renal function by measuring blood urea nitrogen (BUN) and serum creatinine levels. (**D**) Western blot analysis of kidney injury markers KIM-1 and NGAL in renal tissues. GAPDH served as the loading control. (**E**) Flow cytometric analysis of pyroptotic cells in kidney tissue. Dot plots show the percentage of double-positive cells for active caspase-1 and TMR red, representing pyroptotic cells. (**F**) Relative expression level of Malat1 in kidney tissues assessed by RT-qPCR and normalized to GAPDH. Data are presented as mean ± SD. $^{**}P < 0.01$, $^{***}P < 0.001$ compared to the Control group.

of IL-1β and IL-18 were significantly elevated in AKI mice, indicating a heightened inflammatory response (Figure 1B). Furthermore, serum levels of BUN and creatinine were markedly increased, confirming impaired renal function (Figure 1C). Western blotting showed significant upregulation of renal injury markers KIM-1 and NGAL in AKI kidneys (Figure 1D). Flow cytometry revealed a notable increase in caspase-1–dependent pyroptotic cells in the AKI group (Figure 1E), consistent with inflammation-associated cell death. Finally, RT-qPCR analysis showed a significant elevation of Malat1 expression in the AKI group compared with controls (Figure 1F). Together, these data confirm that LPS-induced AKI is associated with inflammation, renal dysfunction, pyroptosis, and upregulation of Malat1.

Malat1 Mitigated Cell Pyroptosis in the LPS-Induced AKI Mouse Model

Lentiviruses containing sh-Malat1 or sh-NC were constructed and administered via tail vein injections in mice to study the association between Malat1 and pyroptosis in an AKI mouse model. The transfection efficiency was validated through RT-qPCR, confirming effective knockdown of Malat1 (Figure 2A). ELISA analysis revealed a significant reduction in pro-inflammatory cytokines IL-1β and IL-18 concentrations after Malat1 knockdown, suggesting decreased inflammation (Figure 2B). Flow cytometry analysis further demonstrated a marked reduction in pyroptosis rate after Malat1 knockdown (Figure 2C). RT-qPCR and immunohistochemistry assays demonstrated a significant downregulation of key pyroptosis-related proteins, such as Caspase-1, GSDMD-N, and NLRP3, in kidney tissues following Malat1 knockdown (Figures 2D–G).

MALAT1 Modulated Inflammation and Pyroptosis in Renal Tubular Epithelial Cells of Mice

To confirm the in vivo effects of Malat1, we transfected sh-Malat1 into LPS-treated TCMK-1 cells, a mouse renal tubular epithelial cell line. RT-qPCR analysis demonstrated a marked decrease in Malat1 expression in TCMK-1 cells, confirming the transfection efficiency of sh-Malat1 (Figure 3A). Furthermore, LPS treatment markedly upregulated Malat1 expression, as shown in Figure 3B. ELISA assays demonstrated that Malat1 knockdown markedly decreased IL-1β and IL-18 pro-inflammatory cytokine protein levels (Figure 3C). Western blot and immunofluorescence analyses demonstrated a significant downregulation of pyroptosis-related markers, including Caspase-1, GSDMD-N, and NLRP3, following Malat1 knockdown (Figures 3D–G).

The m^{6}A-Catalytic Enzyme METTL3 Interacted with MALAT1, and Its Upregulation Was Noted in LPS-Induced AKI Mouse Models

Next, we performed bioinformatics correlation analysis using the STARING and SRAMP tools. The results revealed that Mettl3 interacts with Malat1 (Figure 4A), and Malat1 contains a predicted m^{6}A modification site (Figure 4B). RT-qPCR analysis showed that Mettl3 expression was significantly upregulated in kidney injury tissues (Figure 4C). MeRIP-qPCR assays demonstrated an increase in m^{6}A methylation levels of Malat1 in renal injury tissues (Figure 4D).

Mettl3 Modulated the m^{6}A Modification of Malat1 in Mice

Lentiviruses targeting sh-Mettl3 and sh-NC were injected into the tail veins of mice based on the assigned groups. RT-qPCR assay was performed to confirm the knockdown success rate and efficiency of Mettl3 (Figure 5A). RT-qPCR and MeRIP-qPCR were employed to assess the effects of Mettl3 knockdown on Malat1 expression and methylation levels. The results demonstrated that knocking down Mettl3 significantly decreased Malat1 expression (Figure 5B) and reduced m^{6}A enrichment on Malat (Figure 5C). These findings suggest that Mettl3 modulates Malat1 expression through m^{6}A methylation, and its knockdown leads to diminished Malat1 translation efficiency.

Mettl3 Modulated the Impact of m^{6}A Modification of Malat1 on Pyroptosis in Mice with Sepsis-Induced AKI

Figure 6A demonstrated the successful transfection efficiency of MALAT1 overexpression. Figure 6B highlighted the altered MALAT1 expression in AKI tissues when MALAT1 was overexpressed alongside METTL3 knockdown. ELISA results indicated a significant increase in pro-inflammatory factors, such as IL-1β and IL-18, in the co-transfected group compared to

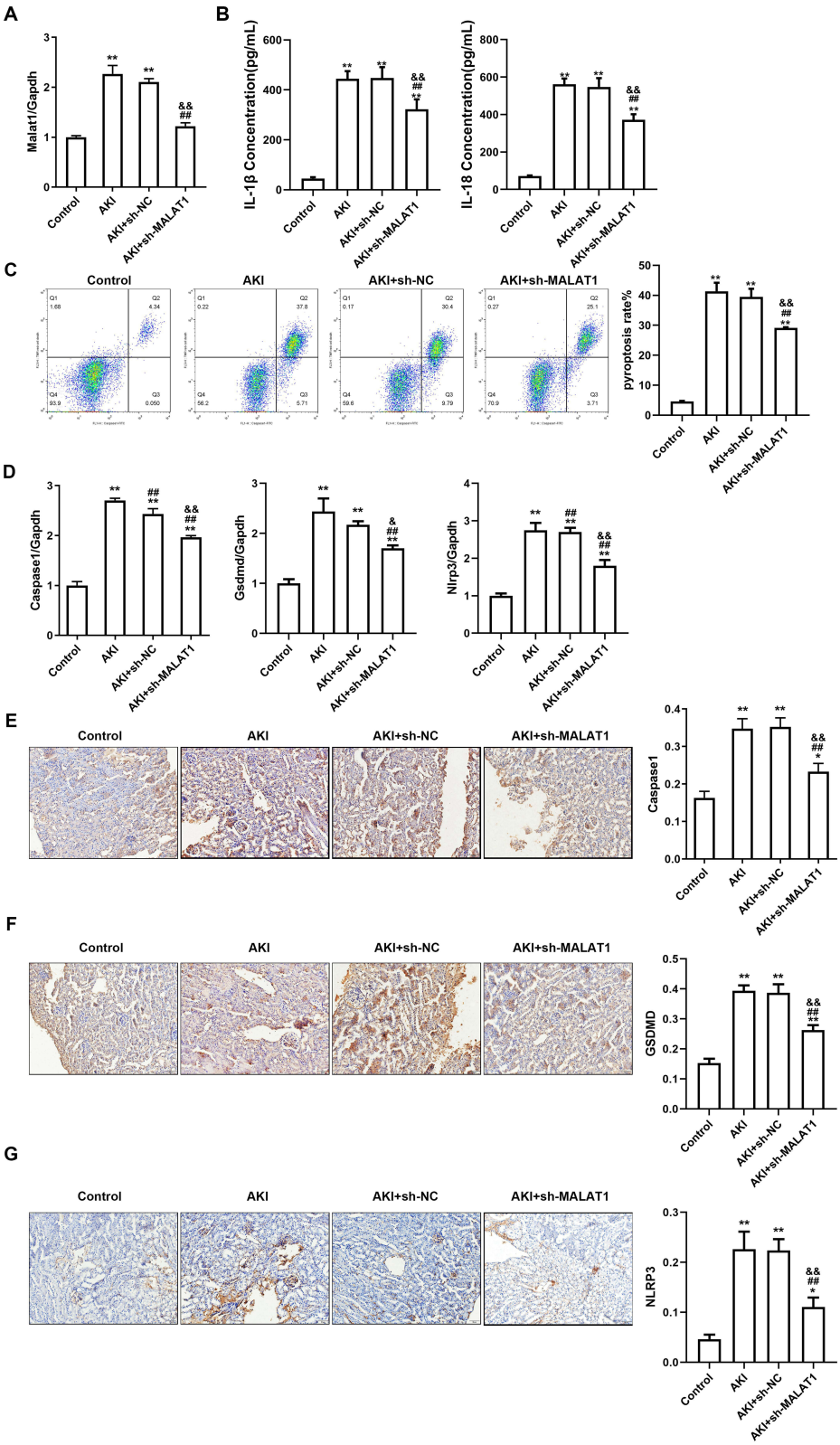

Figure 2 Knockdown of Malat1 alleviates pyroptosis and inflammation in LPS-induced AKI mouse model. (**A**) Quantitative RT-PCR analysis of kidney tissues confirmed successful knockdown of Malat1 expression following administration of Malat1-targeted shRNA via lentiviral vectors. (**B**) Serum levels of pro-inflammatory cytokines IL-1β and IL-18 were measured using ELISA. (**C**) Flow cytometry analysis of renal tissues using caspase-1-FITC and TMR-Red co-staining revealed an increased pyroptotic cell population in AKI mice. (**D**) RT-qPCR quantification of mRNA levels of pyroptosis-related genes including Caspase-1, GSDMD, and NLRP3. (**E-G**) IHC staining of kidney sections to assess protein levels of Caspase-1 (**E**), GSDMD (**F**), and NLRP3 (**G**). Brown DAB staining intensity represents protein expression in tubular epithelial cells. Quantitative analysis (right) confirmed that Malat1 knockdown reduced expression of these pyroptosis markers. All data are presented as mean ± SD. $^{**}P < 0.01$ vs Control group; $^{\#\#}P < 0.01$ vs AKI group; $^{\&}P < 0.05$, $^{\&\&}P < 0.01$ vs AKI+sh-NC group.

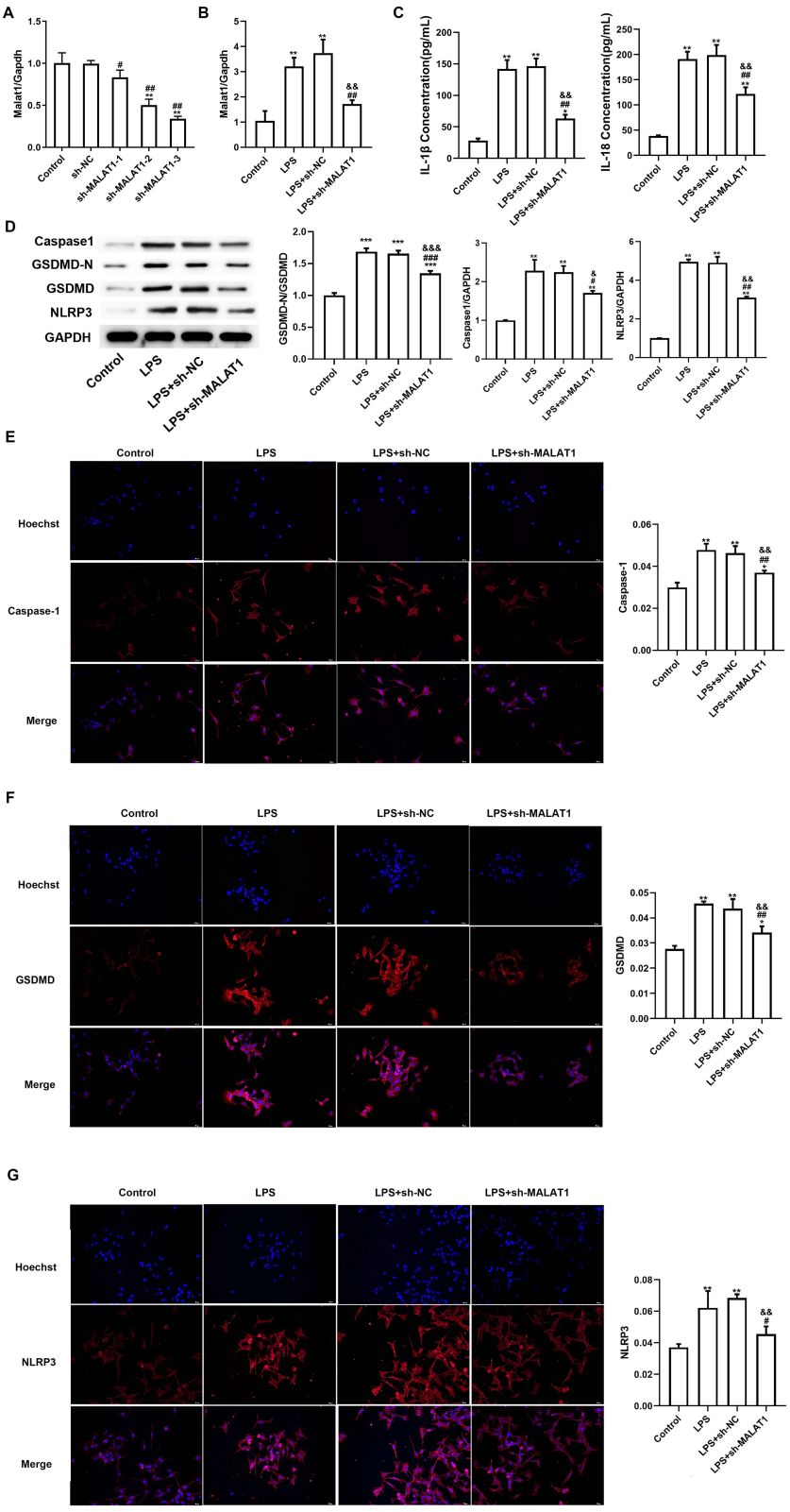

Figure 3 Malat1 regulates inflammation and pyroptosis in LPS-induced injury of mouse renal tubular epithelial cells. (**A**) RT-qPCR was performed to verify the knockdown efficiency of Malat1 in TCMK-1 cells transfected with Malat1-targeting shRNA constructs. (**B**) Quantification of Malat1 expression after LPS stimulation, with or without shRNA transfection. (**C**) ELISA measurements of IL-1β and IL-18 concentrations in the cell supernatant indicated increased inflammation in the LPS group. (**D**) Western blot analysis showing the protein expression levels of pyroptosis-related markers including cleaved GSDMD (GSDMD-N), full-length GSDMD, Caspase-1, and NLRP3, normalized to GAPDH. (**E**–**G**) Immunofluorescence staining of Caspase-1 (**E**), GSDMD (**F**), and NLRP3 (**G**) in TCMK-1 cells following LPS induction, with or without Malat1 knockdown. Red fluorescence indicates protein expression, and Hoechst (blue) labels nuclei. Quantification of fluorescence intensity is shown at right. All experiments were independently repeated three times. $^{*}P < 0.05$, $^{**}P < 0.01$, $^{***}P < 0.001$ vs control group; $^{\#}P < 0.05$, $^{\#\#}P < 0.01$, $^{\#\#\#}P < 0.001$ vs LPS group; $^{\&}P < 0.05$, $^{\&\&}P < 0.01$, $^{\&\&\&}P < 0.001$ vs LPS+sh-NC group.

https://doi.org/10.2147/JIR.S530214

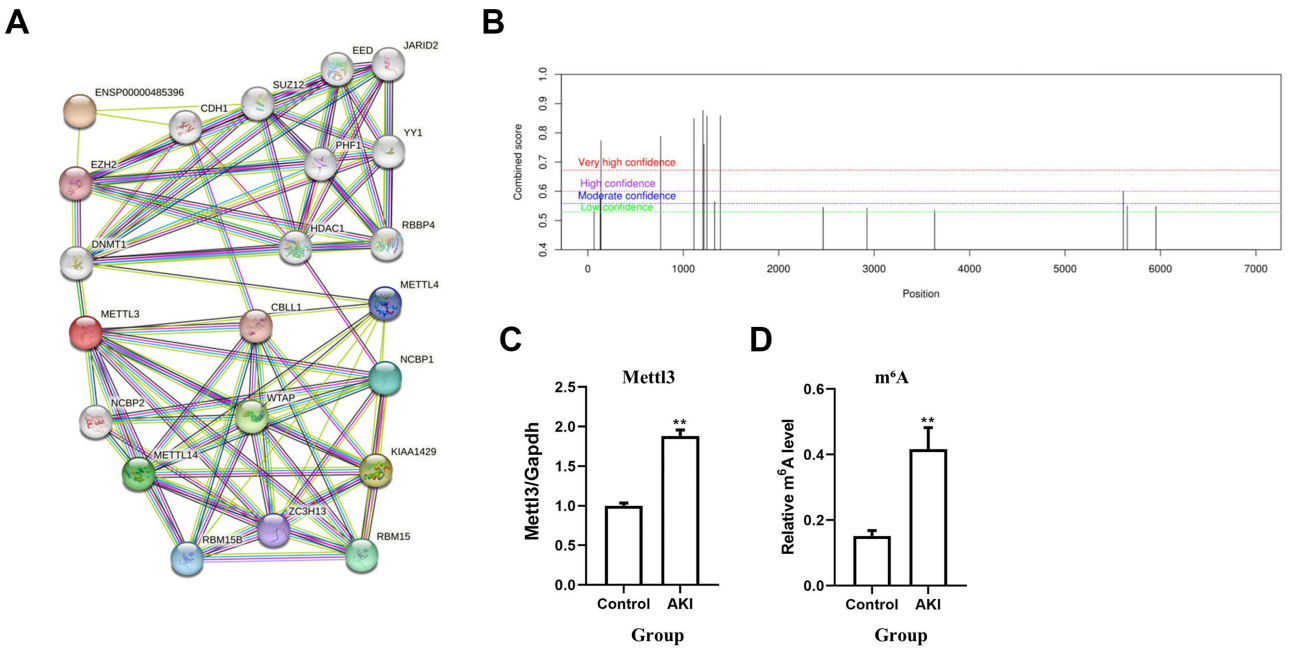

Figure 4 METTL3 is associated with MALAT1 and contributes to increased m^{6}A methylation in LPS-induced AKI mice model. (**A**) Protein-protein interaction (PPI) network of METTL3 and associated m^{6}A regulatory proteins analyzed using the STRING database. MALAT1 (ENSP00000485396) is predicted to interact with METTL3 and several other m^{6}A-related factors, including WTAP, METTL14, and RBM15. (**B**) Predicted m^{6}A methylation sites in the MALAT1 transcript (NR_002847.3) analyzed by SRAMP. The graph illustrates the distribution of m^{6}A sites across the transcript, with confidence levels indicated by different color thresholds. (**C**) RT-qPCR analysis showing significantly elevated expression of Mettl3 in kidney tissues from AKI mice compared to controls. (**D**) Methylated RNA immunoprecipitation followed by qPCR (MeRIP-qPCR) revealed increased m^{6}A modification levels of MALAT1 in the AKI group. All results are expressed as mean ± SD from three independent experiments. $^{**}P < 0.01$ vs Control group.

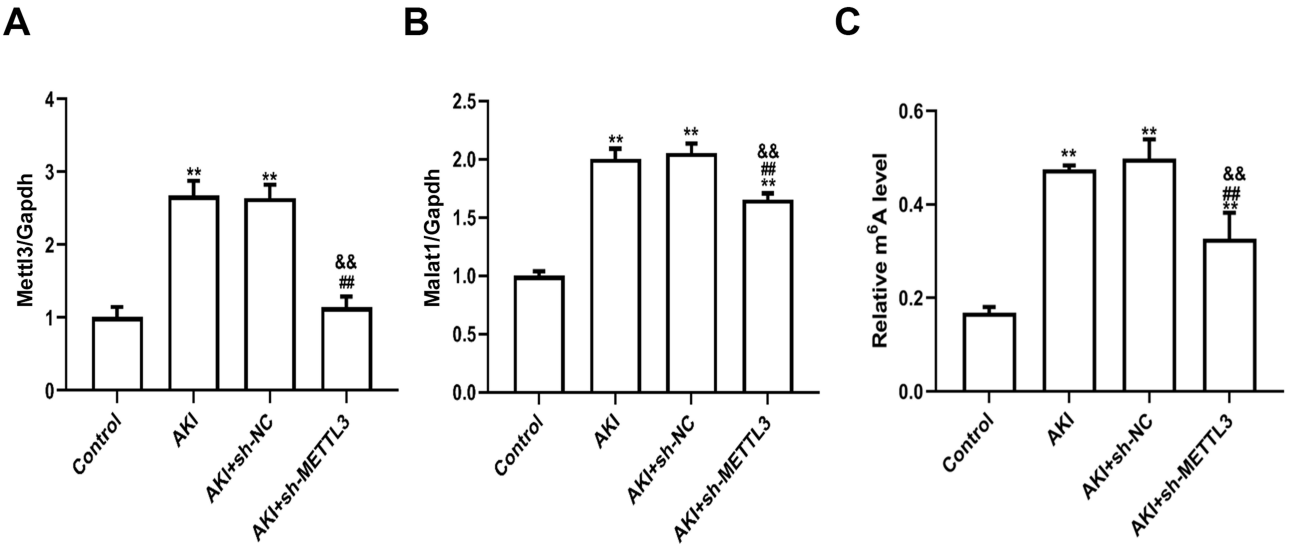

Figure 5 METTL3 regulates m^{6}A modification of MALAT1 in the AKI model. (**A**) RT-qPCR analysis confirmed successful knockdown of METTL3 in kidney tissues from AKI mice. (**B**) RT-qPCR analysis showed that METTL3 knockdown significantly reduced MALAT1 expression levels compared to the AKI and AKI+sh-NC groups. (**C**) MeRIP-qPCR assay revealed that knockdown of METTL3 decreased m^{6}A modification levels of MALAT1 in renal tissues. All results are presented as mean ± SD from three independent experiments. $^{**}P < 0.01$ vs Control group; $^{\#\#}P < 0.01$ vs AKI group; $^{\&\&}P < 0.01$ vs AKI+sh-NC group.

the METTL3 knockdown group alone (Figure 6C). Histological analysis showed that while METTL3 knockdown alleviated renal tissue injury, this protective effect was reversed upon MALAT1 overexpression (Figure 6D). Flow cytometry confirmed that the pyroptosis rate was higher in the co-transfected group compared to METTL3 knockdown alone (Figure 6E). RT-qPCR and immunohistochemistry revealed significant upregulation of pyroptosis markers Caspase-1, GSDMD-N, and NLRP3 upon

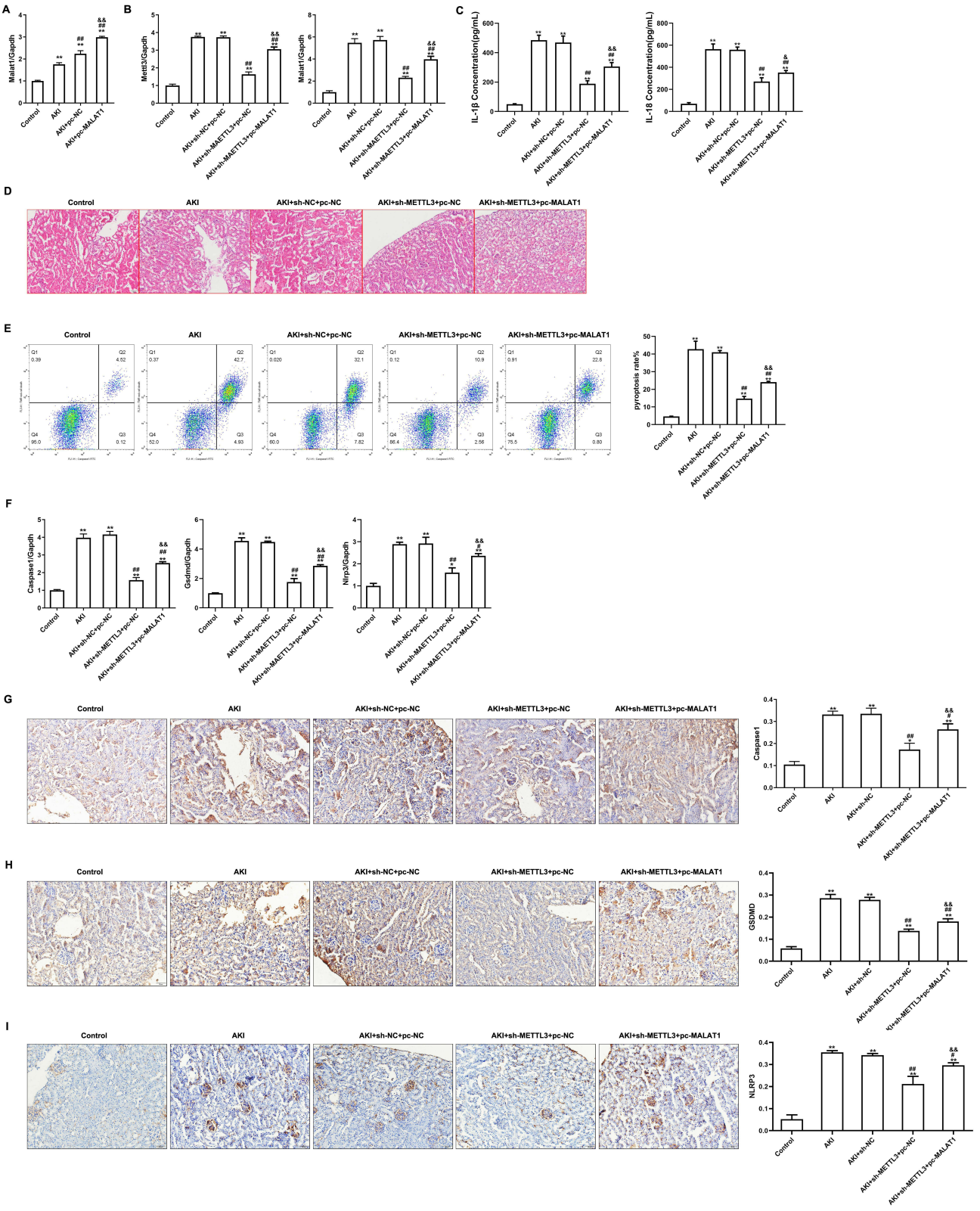

Figure 6 METTL3 modulates the m^{6}A modification of MALAT1 to regulate pyroptosis in a mouse model of LPS-induced AKI. (**A** and **B**) RT-qPCR analysis confirmed the knockdown efficiency of METTL3 and the changes in MALAT1 expression across treatment groups. (**C**) Serum levels of inflammatory cytokines IL-1β and IL-18 were assessed by ELISA to evaluate systemic inflammation. (**D**) Representative HE staining images of kidney sections showing histopathological changes in renal injury. (**E**) Pyroptosis in renal tissues was measured using flow cytometry with active caspase-1 and TMR red double staining. (**F**) mRNA expression levels of pyroptosis-related genes (Caspase-1, GSDMD, and NLRP3) in renal tissues were quantified using RT-qPCR. (**G-I**) Protein expression of Caspase-1, GSDMD, and NLRP3 in kidney tissues was assessed by IHC, with representative images and quantification shown. All results are expressed as mean ± SD from three independent experiments. *$P < 0.05$, **$P < 0.01$ vs Control group; $^{\#}P < 0.05$, $^{\#\#}P < 0.01$ vs AKI group; $^{\&}P < 0.05$, $^{\&\&}P < 0.01$ vs AKI+sh-NC group.

https://doi.org/10.2147/JIR.S530214

concurrent MALAT1 overexpression and METTL3 knockdown (Figure 6F–I). These findings highlight the role of METTL3 and MALAT1 interaction in modulating pyroptosis and inflammation in AKI.

Mettl3 Influenced the m^{6}A Modification Level of Malat1 in vitro

To investigate whether METTL3 modulates MALAT1 expression through m^{6}A RNA methylation, we examined METTL3 and MALAT1 levels in LPS-induced TCMK-1 cells. RT-qPCR revealed that LPS treatment significantly increased METTL3 and MALAT1 expression compared to the control group. Knockdown of METTL3 (LPS+sh-METTL3) markedly reversed these effects relative to LPS+sh-NC (Figure 7A). Furthermore, m^{6}A quantification showed that LPS stimulation elevated global m^{6}A levels, while METTL3 knockdown significantly decreased m^{6}A methylation (Figure 7B). To determine whether METTL3 directly methylates MALAT1, we performed RIP followed by RT-PCR. METTL3 overexpression enhanced the m^{6}A enrichment of MALAT1, whereas METTL3 silencing significantly reduced it (Figure 7C). These findings confirm that METTL3 regulates MALAT1 stability via m^{6}A methylation in SAKI.

Mettl3 Regulated Malat1-Mediated Pyroptosis in AKI Cell Models

Additionally, we investigated pyroptosis-related markers in LPS-treated TCMK-1 cells. Figures 8A and B show the transfection efficiency of Malat1 overexpression and Mettl3 knockdown in TCMK-1 cells. ELISA results indicated that

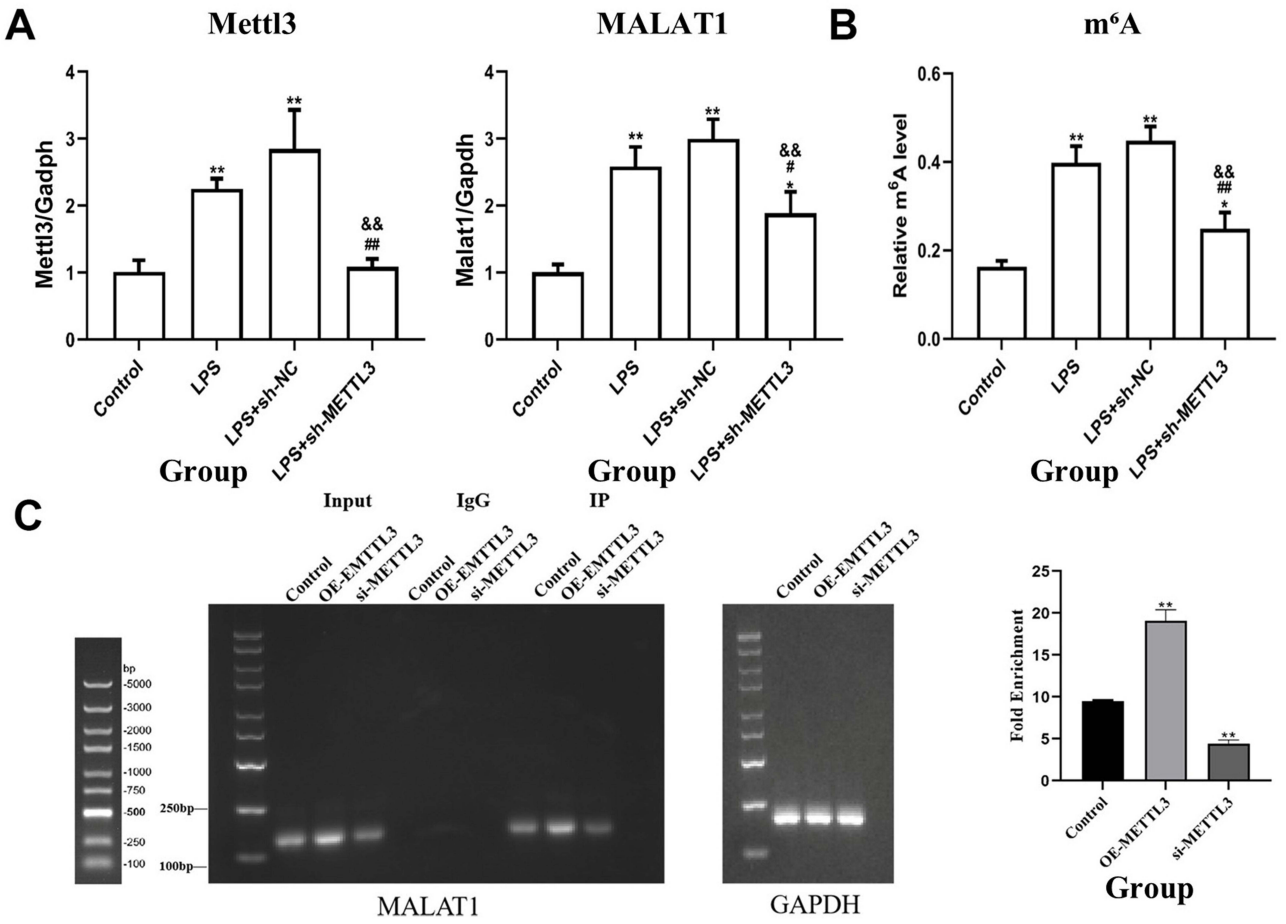

Figure 7 METTL3 regulates the m^{6}A methylation of MALAT1 in vitro under LPS stimulation. (**A**) The mRNA expression levels of METTL3 and MALAT1 were measured in mouse renal tubular epithelial cells (TCMK-1) using RT-qPCR following LPS treatment and lentiviral transfection with sh-METTL3 or negative control (sh-NC). (**B**) The m^{6}A modification level of MALAT1 was determined using MeRIP-qPCR. (**C**) RIP-PCR and RT-qPCR showing METTL3-mediated m^{6}A enrichment of MALAT1. Representative gel electrophoresis images of MALAT1 and GAPDH (negative control) immunoprecipitated by anti-m^{6}A antibody are shown. The bar graph on the right presents fold enrichment of MALAT1 in METTL3 overexpression (OE-METTL3) and knockdown (si-METTL3) groups relative to control. All data are expressed as mean ± SD based on three independent experiments. $^*P < 0.05$, $^{**}P < 0.01$ vs Control group; $^{\#}P < 0.05$, $^{\#\#}P < 0.01$ vs LPS group; $^{\&\&}P < 0.01$ vs LPS+sh-NC group.

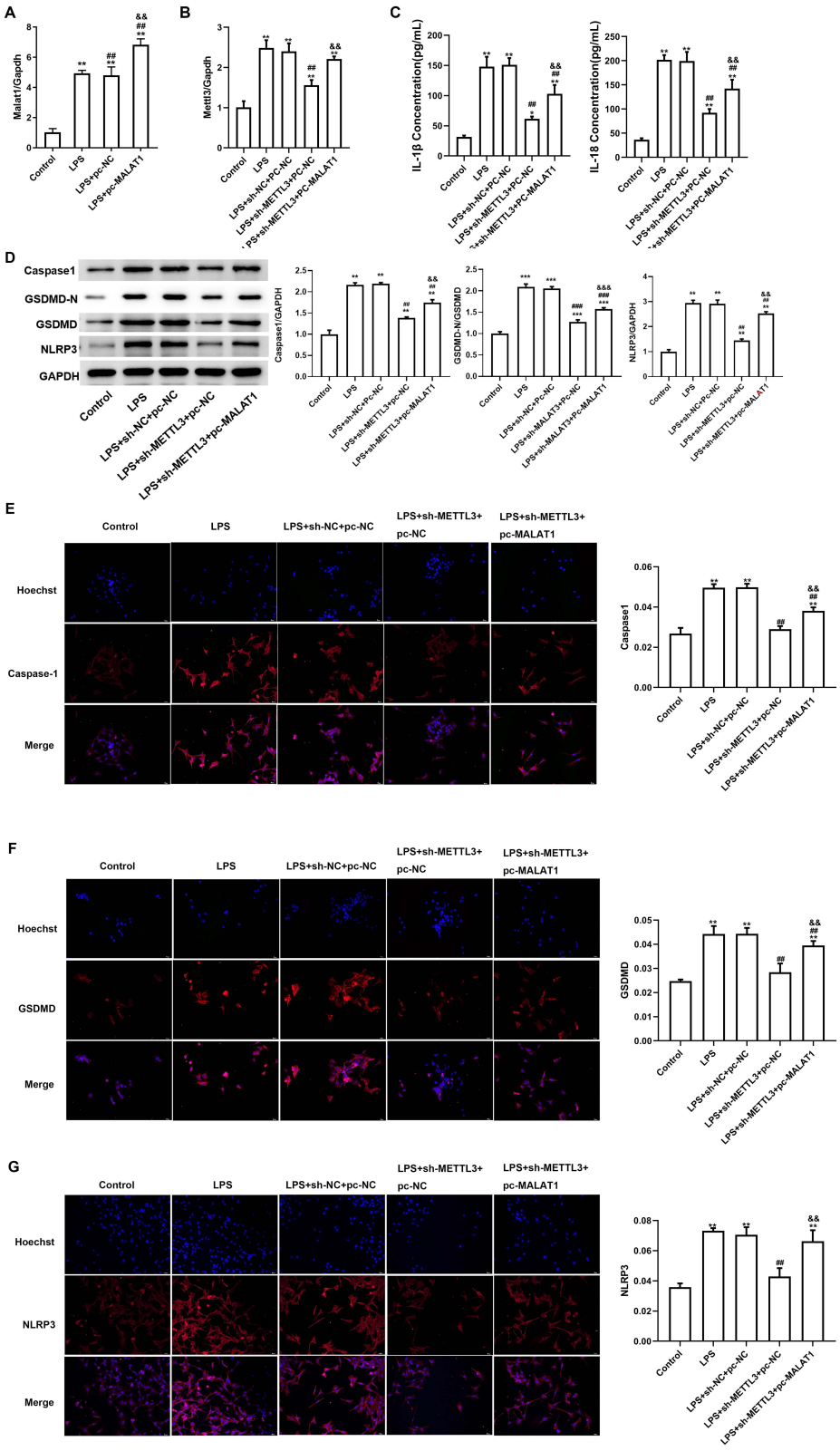

Figure 8 METTL3 regulates MALAT1-mediated pyroptosis in an LPS-induced AKI cell model. (**A** and **B**) RT-qPCR analysis of METTL3 and MALAT1 expression in mouse renal tubular epithelial cells (TCMK-1) treated with LPS and transfected with sh-METTL3 and/or MALAT1 overexpression plasmid (pc-MALAT1). (**C**) Quantification of inflammatory cytokines IL-1β and IL-18 in the cell supernatants using ELISA. (**D**) Western blot analysis of pyroptosis-related proteins including Caspase-1, GSDMD, GSDMD-N, and NLRP3. (**E-G**) Immunofluorescence staining of Caspase-1 (**E**), GSDMD (**F**), and NLRP3 (**G**) to visualize and quantify protein expression levels in different treatment groups. Nuclear staining was performed using Hoechst 33342. Quantitative bar graphs for each immunofluorescence panel are shown on the right. Data represent mean ± SD of three independent experiments. $^{*}P < 0.05$, $^{**}P < 0.01$, $^{***}P < 0.001$ vs Control group; $^{\#\#}P < 0.01$, $^{\#\#\#}P < 0.001$ vs LPS group; $^{\&\&}P < 0.01$, $^{\&\&\&}P < 0.001$ vs LPS+sh-NC+pc-NC group.

https://doi.org/10.2147/JIR.S530214

Mettl3 knockdown significantly decreased inflammatory factor levels in the cell supernatant, but this reduction was reversed with Malat1 overexpression (Figure 8C). Western blot and immunofluorescence analyses demonstrated that Mettl3 knockdown significantly reduced the expression of pyroptosis-related markers (NLRP3, GSDMD-N, and Caspase-1), whereas Malat1 overexpression led to an increase in these markers (Figures 8D–G).

Discussion

SAKI is a critical condition with high morbidity and mortality, characterized by inflammation-driven renal dysfunction.[2,3] In this study, we identified the long non-coding RNA Malat1 as a key player in promoting renal inflammation and pyroptosis in SAKI. Using both in vivo and in vitro models, we found that Malat1 expression was significantly upregulated in response to LPS-induced injury, coinciding with increased inflammatory cytokine levels, pyroptotic cell death, and histological damage in kidney tissues.

In details, structural analysis of kidney tissues in AKI mice showed notable damage, such as renal tubular epithelial cell loss and cytoplasmic vacuolation, along with elevated pro-inflammatory cytokines IL-1β and IL-18, indicating strong inflammation. These observations were accompanied by an elevated pyroptosis rate, which was confirmed through flow cytometry. Malat1 expression was notably increased in kidney tissues of LPS-induced AKI mice, indicating its potential involvement in inflammatory response and cell death during renal injury. In previous studies, Lu et al and Wang et al also found that MALAT1 could promote AKI progression and inflammation response,[14,15] which were consistent with our results, and strengthened the credibility of our study. To further assess the role of MALAT1 in pyroptosis and inflammation, we knocked down Malat1 in vivo using lentiviral shRNA constructs. Our findings indicate that Malat1 knockdown decreases inflammatory cytokine levels and significantly lowers the pyroptosis rate in kidney cells, as shown by reduced expression of key pyroptotic markers, including Caspase-1, GSDMD, and NLRP3. The decrease in pyroptosis was associated with enhanced kidney function, as demonstrated by histological and biochemical assessments. These findings indicate that increased MALAT1 expression is significantly linked to heightened inflammatory responses and pyroptosis in the kidney during AKI. In vitro experiments with TCMK-1, a mouse renal tubular epithelial cell line, confirmed our in vivo findings. LPS treatment significantly upregulated Malat1 expression, while Malat1 knockdown decreased inflammatory cytokine levels and pyroptosis-related protein expression in cells. These findings highlight Malat1's pro-inflammatory and pro-pyroptotic role in renal tubular epithelial cells during AKI.

Furthermore, we examined the potential regulatory mechanisms that could mediate MALAT1's effects. Bioinformatics analysis revealed that METTL3, an m^6A methyltransferase, interacts with MALAT1 and contributes to the regulation of its expression. For more than 50 years, RNA modifications have been recognized for their impact on RNA structure and function.[18] m^6A modification is a common and essential regulator of RNA metabolism, influencing pre-mRNA processing, translation efficiency, transcript stability, and miRNA biogenesis.[19] METTL3, the initially discovered methyltransferase, primarily catalyzes m6A modifications on mRNAs and non-coding RNAs.[20,21] Recent research underscores METTL3's involvement in various cancers, such as gastric, colon, lung, and osteosarcoma.[20,21] However, the roles of METTL3 in AKI or even SAKI remains unclear. Importantly, our data revealed that METTL3, a core component of the m^6A RNA methylation machinery, modulates the stability and expression of Malat1 via m^6A-dependent mechanisms. RIP and MeRIP-qPCR assays confirmed the binding of METTL3 to Malat1 and demonstrated altered m^6A modification levels under different METTL3 expression conditions. Functional experiments further showed that METTL3 knockdown led to a reduction in Malat1 expression and subsequent inhibition of Caspase-1, GSDMD, and NLRP3 activation, highlighting METTL3's upstream regulatory role in Malat1-mediated pyroptosis. Moreover, cleaved GSDMD (GSDMD-N), a hallmark of pyroptotic execution,[23,24] was measured and shown to be significantly downregulated upon METTL3 or Malat1 silencing, affirming their contribution to pyroptosis. The use of both flow cytometry and immunohistochemistry supported the conclusion that pyroptosis was a major pathophysiological process in SAKI.

Our results are consistent with emerging studies linking epigenetic regulation to innate immune activation in renal injury. The METTL3-Malat1 axis represents a novel regulatory pathway that integrates m^6A epitranscriptomic signaling with inflammasome activation. These findings expand current understanding of the molecular mechanisms driving SAKI and suggest that targeting METTL3 or disrupting Malat1 m6A modifications may offer therapeutic potential.

However, several limitations of this study should be acknowledged. First, although METTL3 and MALAT1 expression were examined in TCMK-1 in vitro, their specific cellular localization in vivo was not directly confirmed. As the lentivirus was systemically administered via tail vein injection, we inferred predominant infection in tubular epithelial cells based on phenotypic outcomes; however, infection efficiency and cell-type specificity were not directly evaluated. Future studies incorporating reporter constructs or immunofluorescence co-staining are necessary to verify lentiviral tropism within renal tissues. Second, while we demonstrated that METTL3 regulates MALAT1 through m^6A modification, other components of the m^6A regulatory machinery—including additional writers, erasers, and readers—may also contribute to the observed effects and were not explored. Third, we did not assess macrophage infiltration or other immune cell dynamics in the kidney, which may play important roles in the inflammatory microenvironment of SAKI. Lastly, m^6A-seq was not performed to provide a transcriptome-wide profile of m6A-modified sites on MALAT1 and other RNAs, limiting a more comprehensive understanding of METTL3's epitranscriptomic functions.

Conclusion

In summary, our findings demonstrate that METTL3-mediated m^6A modification enhances Malat1 stability, thereby promoting pyroptosis and inflammation in SAKI. By systematically dissecting this regulatory axis, we reveal a previously unrecognized mechanism of renal injury and identify METTL3 as a potential upstream target for therapeutic intervention. While our study primarily focused on METTL3 knockdown, its functional dominance over Malat1 in this context highlights its central role in driving disease progression.

Data Sharing Statement

The datasets generated or analyzed during this-study are-available from corresponding author (yanfei.ma@ymun.edu.cn) on reasonable request.

Ethics Statement

Animal experiments received approval from Zhuoqiang Biotechnology Co., Ltd (No.: zqia-2023-027).

Author Contributions

All authors made a significant contribution to the work reported, whether that is in the conception, study design, execution, acquisition of data, analysis and interpretation, or in all these areas; took part in drafting, revising or critically reviewing the article; gave final approval of the version to be published; have agreed on the journal to which the article has been submitted; and agree to be accountable for all aspects of the work.

Funding

This study was supported by Guangxi Natural Science Foundation (No.:2025GXNSFHA069037); Guangxi Zhuang Autonomous Region Administration of Traditional Chinese Medicine 2023 Self-financed Research Topics in Traditional Chinese Medicine (No.: GXZYL20230364); Guangxi Zhuang Autonomous Region Health and Wellness Commission 2023 Guangxi Zhuang Autonomous Region Health and Wellness Commission Self-financed Scientific Research Topics in Western Medicine Category (No.: Z-L20230874); Research Program for High-level Talents of Affiliated Hospital of Youjiang Medical University For Nationalities (No.: y202011719); Baise City Scientific Research and Technology Development Program Self-financing Subjects (No.: baizi20220915).

Disclosure

The authors have no conflicts of interest to declare.

References

1. Singer M, Deutschman CS, Seymour CW, et al. The third international consensus definitions for sepsis and septic shock (Sepsis-3). *JAMA*. 2016;315:801–810. doi:10.1001/jama.2016.0287
2. Poston JT, Koyner JL. Sepsis associated acute kidney injury. *BMJ*. 2019;364:k4891. doi:10.1136/bmj.k4891

3. Mayeux PR, MacMillan-Crow LA. Pharmacological targets in the renal peritubular microenvironment: implications for therapy for sepsis-induced acute kidney injury. *Pharmacol Ther*. 2012;134:139–155. doi:10.1016/j.pharmthera.2012.01.004
4. Chang YM, Chou YT, Kan WC, Shiao CC. Sepsis and acute kidney injury: a review focusing on the bidirectional interplay. *Int J Mol Sci*. 2022;23. doi:10.3390/ijms23169159
5. Sanz AB, Sanchez-Nino MD, Ramos AM, Ortiz A. Regulated cell death pathways in kidney disease. *Nat Rev Nephrol*. 2023;19:281–299. doi:10.1038/s41581-023-00694-0
6. Wu Z, Deng J, Zhou H, Tan W, Lin L, Yang J. Programmed cell death in sepsis associated acute kidney injury. *Front Med*. 2022;9:883028. doi:10.3389/fmed.2022.883028
7. Rao Z, Zhu Y, Yang P, et al. Pyroptosis in inflammatory diseases and cancer. *Theranostics*. 2022;12:4310–4329. doi:10.7150/thno.71086
8. Lin J, Cheng A, Cheng K, et al. New insights into the mechanisms of pyroptosis and implications for diabetic kidney disease. *Int J Mol Sci*. 2020;21:7057. doi:10.3390/ijms21197057
9. Yu P, Zhang X, Liu N, Tang L, Peng C, Chen X. Pyroptosis: mechanisms and diseases. *Signal Transduct Target Ther*. 2021;6:128. doi:10.1038/s41392-021-00507-5
10. Sun J, Ge X, Wang Y, Niu L, Tang L, Pan S. USF2 knockdown downregulates THBS1 to inhibit the TGF-beta signaling pathway and reduce pyroptosis in sepsis-induced acute kidney injury. *Pharmacol Res*. 2022;176:105962. doi:10.1016/j.phrs.2021.105962
11. Nemeth K, Bayraktar R, Ferracin M, Calin GA. Non-coding RNAs in disease: from mechanisms to therapeutics. *Nat Rev Genet*. 2024;25:211–232. doi:10.1038/s41576-023-00662-1
12. Ignarski M, Islam R, Muller RU. Long non-coding RNAs in kidney disease. *Int J Mol Sci*. 2019;20:3276. doi:10.3390/ijms20133276
13. Kolling M, Genschel C, Kaucsar T, et al. Hypoxia-induced long non-coding RNA Malat1 is dispensable for renal ischemia/reperfusion-injury. *Sci Rep*. 2018;8:3438. doi:10.1038/s41598-018-21720-3
14. Lu HY, Wang GY, Zhao JW, Jiang HT. Knockdown of lncRNA MALAT1 ameliorates acute kidney injury by mediating the miR-204/APOL1 pathway. *J Clin Lab Anal*. 2021;35:e23881. doi:10.1002/jcla.23881
15. Wang B, Wang Y, Xu K, et al. Resveratrol alleviates sepsis-induced acute kidney injury by deactivating the lncRNA MALAT1/MiR-205 axis. *Cent Eur J Immunol*. 2021;46:295–304. doi:10.5114/ceji.2021.109195
16. Shu B, Zhou YX, Li H, Zhang RZ, He C, Yang X. The METTL3/MALAT1/PTBP1/USP8/TAK1 axis promotes pyroptosis and M1 polarization of macrophages and contributes to liver fibrosis. *Cell Death Discov*. 2021;7:368. doi:10.1038/s41420-021-00756-x
17. Zeng M, Chen Z, Wang Y, et al. LncRNA MALAT1 to enhance pyroptosis in viral myocarditis through UPF1-mediated SIRT6 mRNA decay and wnt-beta-catenin signal pathway. *Cardiovasc Toxicol*. 2024;24:1439–1454. doi:10.1007/s12012-024-09922-w
18. Roundtree IA, Evans ME, Pan T, He C. Dynamic RNA modifications in gene expression regulation. *Cell*. 2017;169:1187–1200. doi:10.1016/j.cell.2017.05.045
19. An Y, Duan H. The role of m6A RNA methylation in cancer metabolism. *Mol Cancer*. 2022;21:14. doi:10.1186/s12943-022-01500-4
20. Jiang X, Liu B, Nie Z, et al. The role of m6A modification in the biological functions and diseases. *Signal Transduct Target Ther*. 2021;6:74. doi:10.1038/s41392-020-00450-x
21. Sendinc E, Shi Y. RNA m6A methylation across the transcriptome. *Mol Cell*. 2023;83:428–441. doi:10.1016/j.molcel.2023.01.006
22. Pan X, Zhou T, Tai YH, et al. Elevated expression of CUEDC2 protein confers endocrine resistance in breast cancer. *Nat Med*. 2011;17:708–714. doi:10.1038/nm.2369
23. Shi J, Zhao Y, Wang K, et al. Cleavage of GSDMD by inflammatory caspases determines pyroptotic cell death. *Nature*. 2015;526:660–665. doi:10.1038/nature15514
24. Du G, Healy LB, David L, et al. ROS-dependent S-palmitoylation activates cleaved and intact gasdermin D. *Nature*. 2024;630:437–446. doi:10.1038/s41586-024-07373-5